Lattice-Boltzmann modeling of a turbulent bluff-body stabilized flame

M. Tayyab, S. Zhao, Pierre Boivin

Lattice-Boltzmann modelling of a turbulent bluff-body stabilized flame

M. Tayyab,[1] S. Zhao,[1,2] and P. Boivin[1, a)]
[1)] *Aix Marseille Univ, CNRS, Centrale Marseille, M2P2, 13451, Marseille, France*
[2)] *CNES launchers directorate, 75612, Paris, France*

(Dated: 19 January 2021)

This letter reports the first large eddy simulation of a turbulent flame using a Lattice-Boltzmann model. To that end, simulation of a bluff-body stabilized propane-air flame is carried out, showing an agreement similar to those available in the literature. Computational costs are also reported, indicating that Lattice-Boltzmann modelling of reactive flows is competitive, with around 1000cpuh required to simulate one residence time in the 1,5m burner.

Lattice-Boltzmann methods (LBM) are an active topic of investigation in the computational fluid dynamics field. In the past decade, they led to unprecedented results in the field of low-Mach, isothermal, aerodynamics and aeroacoustics. The two main ingredients of this success can be summarized as follows. (i) LBM is highly scalable and HPC friendly by nature, due to its stream and collide algorithm[1,2]. In practice, CPU costs are reportedly divided by 5 to 10 compared to conventional Navier-Stokes solvers. (ii) Besides being second-order accurate in time and space[1], LBM presents excellent dissipation properties for pressure waves, comparable with high-order methods[3]. Owing to this success, there is today an unprecedented effort in extending those methods to tackle problems beyond low-Mach athermal flows: compressible flows[4,5], reactive flows[6–8], multiphase flows[9].

Our group recently presented a pressure-based LB model designed to cope with both high Mach flows[10] and reactive flows[11], emerging from earlier studies[4,7,8]. These studies validated the behavior of the model on standard combustion test cases, including, e.g. laminar flame propagation[7,8], counterflow diffusion flame[8], vortex/flame interactions[7], diffusion flame stabilized in double shear layer[7], and thermo-diffusive instabilities[11]. This letter aims at proving the method to be also suitable for more complex configurations, through investigation of a premixed turbulent flame. To that end, we selected the so-called VOLVO burner, for which a rich experimental database exists[12,13]. The test case, consisting of a premixed turbulent flame stabilized behind a bluff-body, has been extensively used to test and tune new turbulent combustion models[14,15].

From the numerical modelling standpoint, many studies have been conducted on the VOLVO burner. Because of its dimensions (1,5m in length), Direct Numerical Simulation (DNS) is out of reach. Reynolds Averaged Navier-Stokes (RANS) simulations were carried out by many researchers[16], but the strategy has been reported to create divergences in the solution[17,18]. To capture the unsteady shedding and vortices breakdown created by the bluff-body, Large Eddy Simulation (LES) presents an attractive alternative, and was adopted in a large number of numerical studies[19–24]. To the authors' knowledge, however, this simulation was never attempted using LBM.

The numerical simulations are carried out with the PROLB software using a pressure-based Lattice Boltzmann (LB) model[10] coupled with a Finite Differences (FD) solver.

In the LB solver, the probability density function f_i (of finding gas particles at x with velocity $\boldsymbol{c}_i$) is solved using a hybrid regularized collision model[7,25]. The streaming and collision process can be expressed under discrete form as

$$\begin{aligned} f_i(t+\delta t,\boldsymbol{x}) &= f_i^{\mathrm{col}}(t,\boldsymbol{x}-\boldsymbol{c_i}\delta t),\\ f_i^{\mathrm{col}}(t,\boldsymbol{x}) &= f_i^{\mathrm{eq}} + \left(1-\frac{\delta t}{\overline{\tau}}\right) f_i^{\mathrm{neq}} + \frac{\delta t}{2} F_i^E \end{aligned} \tag{1}$$

where δt is the time-step, $\boldsymbol{c}_i$ is the i^{th} discrete velocity of the D3Q19 lattice set, f_i^{eq} and f_i^{neq} the equilibrium and non-equilibrium segments of the distribution function and F_i^E is the forcing term required to correctly recover the stress tensor[4,7]. $\bar{\tau}$ is a non-dimensional relaxation time depending on the dynamic viscosity ν as

$$\overline{\tau} = \frac{\nu}{c_s^2} + \frac{\delta t}{2} \tag{2}$$

where c_s is the lattice sound speed. Full expressions for f_i^{eq}, f_i^{neq}, F_i^E and their relation with the macroscopic variables are provided as supplementary material. They correspond[10] to solving the following macroscopic equations

$$\frac{\partial \rho}{\partial t} + \frac{\partial \rho u_\beta}{\partial x_\beta} = 0,, \tag{3a}$$

$$\frac{\partial \rho u_\alpha}{\partial t} + \frac{\partial \rho u_\alpha u_\beta + p\delta_{\alpha\beta} - \mathscr{T}_{\alpha\beta}}{\partial x_\beta} = 0\,, \tag{3b}$$

where ρ is the volume mass, u_α is the local velocity vector and p is the pressure, obeying the multi-component perfect gas law. $\mathscr{T}_{\alpha\beta}$ is the stress tensor,

$$\mathscr{T}_{\alpha\beta} = \rho\nu\left(\frac{\partial u_\alpha}{\partial x_\beta} + \frac{\partial u_\beta}{\partial x_\alpha} - \delta_{\alpha\beta}\frac{2}{3}\frac{\partial u_\gamma}{\partial x_\gamma}\right). \tag{4}$$

The FD solver coupled with the above is responsible for solving species and energy conservation. For each species k,

$$\rho\frac{\partial Y_k}{\partial t} + \rho u_\alpha \frac{\partial Y_k}{\partial x_\alpha} = \frac{\partial}{\partial x_\alpha}(-\rho Y_k V_{k,\alpha}) + \dot{\omega}_k\,, \tag{5}$$

where Y_k is the mass fraction of species k, $\dot{\omega}_k$ is its net chemical production rate , and $V_{k,\alpha}$ the diffusion velocity[26]. In this

[a)] Electronic mail: pierre.boivin@univ-amu.fr

work, the energy conservation is solved in its enthalpy form[26]

$$h = \sum_{k=1}^{N} h_k Y_k \ , \ h_k = \int_{T_0}^{T} C_{p,k}(T)dT + \Delta h^0_{f,k}, \tag{6}$$

where T and h are linked through NASA polynomials leading to the following enthalpy equation

$$\rho \frac{\partial h}{\partial t} + \rho u_\alpha \frac{\partial h}{\partial x_\alpha} = \frac{Dp}{Dt} - \frac{\partial q_\alpha}{\partial x_\alpha} + \mathscr{T}_{\alpha\beta} \frac{\partial u_\alpha}{\partial x_\beta}, \tag{7}$$

where $\frac{Dp}{Dt} = \frac{\partial p}{\partial t} + u_\alpha \frac{\partial p}{\partial x_\alpha}$ is neglected. The heat flux q_α reads

$$q_\alpha = -\lambda \frac{\partial T}{\partial x_\alpha} + \rho \sum_{k=1}^{N} h_k Y_k V_{k,\alpha}, \tag{8}$$

with λ the thermal conductivity. Diffusion velocities are defined as in[7], using constant Schmidt number for each species, and a correction velocity to ensure mass conservation[26].

The possible spatial discretization being much larger than the smallest flow structures, subgrid modelling is required. First, a turbulent model is implemented for the flow, coming down to modifying the dynamic viscosity in the momentum equation (3b) as $\nu \to \nu + \nu_t$, where ν_t is the turbulent Vremann model[27] available in PROLB, a model validated for a wide range of applications covering external aerodynamics to urban flows[25,28]. Turbulent Schmidt and Prandtl numbers are introduced[26], to modify accordingly the transport properties in Eqs. (5, 8).

Lastly, the flame is thickened via the dynamic thickened flame large eddy simulation (TFLES) model[22,29]. To account for flame/turbulence interactions at the subgrid level, the model consists in modifying the flame structure locally in two steps:

Step 1: Thickening of the flame by a factor F,

Step 2: Applying an efficiency function $\mathscr{E}$, as proposed by Charlette et al.[30,31], to enhance the transport and kinetics where the flame is highly wrinkled.

In practice, applying this model corresponds to multiplying all transport terms by $\mathscr{E}F$, and kinetic source terms by $\mathscr{E}/F$; only where a flame sensor S is activated. The corresponding species and energy filtered equations are recalled in the supplementary material. S and $\mathscr{E}$ are obtained following Rochette's proposal[29].

The VOLVO burner[12,13] consists of a rectangular box of dimensions $(L_x, L_y, L_z) = 1.55\text{m} \times 0.12\text{m} \times 0.24\text{m}$ (see the choice of axes in Fig. 1). In its center lies a bluff-body of equilateral triangular cross section of dimension $D = 0.04$m. The region upstream the flame holder consists of air and fuel injectors along with a honeycomb structure to obtain a turbulent premixed mixture of propane and air. Following other studies[22,29,32], the numerical setup is simplified to a propane-air turbulent inlet (without injectors or honeycomb). Dimensions of the numerical burner are provided in Fig. 1. In the experiment, top and bottom walls (in the y direction) are water cooled, while side walls (in the z direction) are air cooled. RMS and mean values of velocity and temperatures are reported[13] for various x- isolines on the centerline $z = 0$, identified in Fig. 1. Velocity profiles are also available along the centerline $y = z = 0$.

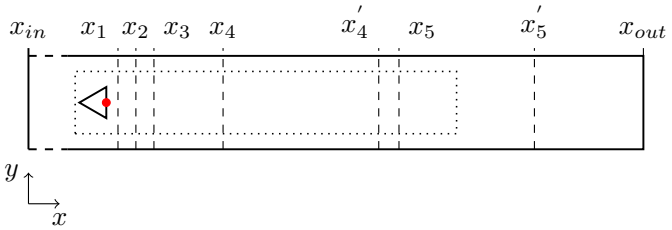

	x_{in}	x_1	x_2	x_3	x_4	x_4'	x_5	x_5'	x_{out}
[mm]	-810	15	38	61.2	150	350	376	550	690

FIG. 1. A Mid-plane cut view of the domain in z-direction is presented, indicating all the positions where measurements are available. The axes origin is identified as the red dot. The dimension of the equilateral triangle is $D = 0.04$m, spanning throughout the width of the burner. The dotted lines indicate the location of the refined region for Case B.

The operating points (equivalence ratio φ, bulk velocity U_b, temperature T_0 and Reynolds number Re) listed in Tab. I are considered in the following, to allow comparison with available numerical studies[22,29]. These conditions were selected for no thermo-acoustic instability is expected[13], while some conditions are reportedly unstable[32].

TABLE I. VOLVO burner operating conditions[12,13] selected for this study, where $\nu = 1.49 \times 10^{-5}\text{m}^2/\text{s}$.

Case	ϕ	U_b(m/s)	T_0(K)	Re=$U_b D/\nu$
Cold	0.65	16.6	288.0	45000.0
Reactive	0.65	17.3	288.0	47000.0

Numerical boundary conditions are specified as follow.

Turbulent velocity inlet: prescribed velocity U_b with a turbulence intensity of 8%, generated using the Random Flow Generation (RFG) technique[33].

No-slip adiabatic walls: top, bottom and bluff-body walls (along the y-direction).

Periodic conditions: in the z-direction. Note that no-slip adiabatic conditions were also considered for these walls, with results presented in Fig. 2.f.

Non-reflective characteristic boundary condition: outlet, with a target pressure of 1atm.

All thermo-chemical properties were taken from earlier studies[22,29]: a two/step propane-air mechanism is considered, with constant Prandtl and species Schmidt numbers, with details provided as supplementary material.

For both the hot and cold configurations, two different meshes (Case A, Case B) are considered.

Case A: Uniform mesh, with spatial resolution $\delta x = 2.0$ mm, resulting in 5.5×10^6 grid points.

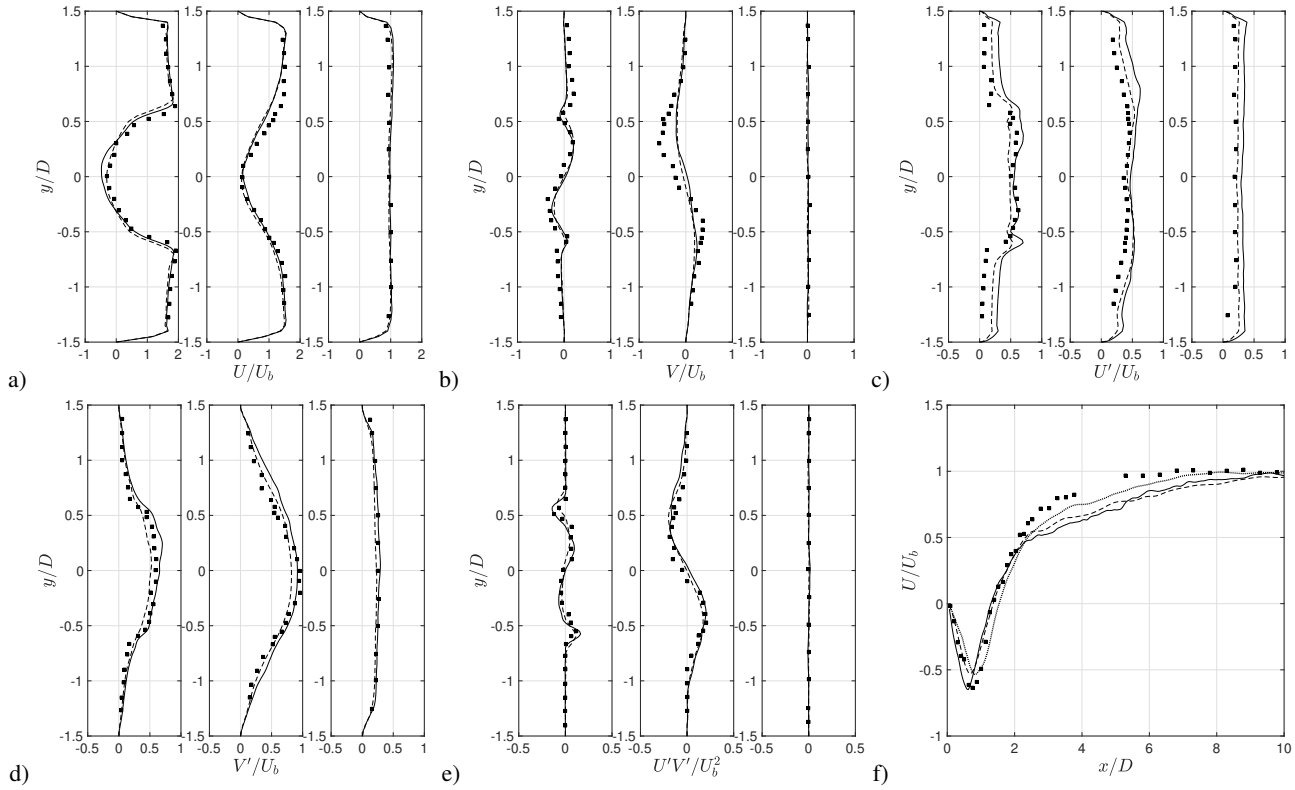

FIG. 2. Quantitative comparisons of our results for the cold flow, at two different grid definitions, with experimental data at five different points (x_1, x_3, x_5) (from left to right of each sub-figure). a) Mean U profiles. b) Mean V profiles. c) RMS U profiles. d) RMS V profiles. e) RMS UV profiles. Case A (dashed line), Case B (solid line) and experimental data (solid square) f) Mean axial velocity profiles starting from the bluff body. Periodic boundaries on the sides (z-direction). Case A (solid line), Case B (dashed line), wall boundaries Case A (dotted line) and experimental data (black solid square).

Case B: Starting from the case A mesh, the region of interest is refined with $\delta x = 1.0$mm (see the dotted lines in Fig. 1), resulting in 17.5×10^6 points.

The time step used is $\delta t = 1.05 \times 10^{-6}$s for the $\delta x = 2$mm region (with the time-step halved in the refined region). For each simulation, three convective times $t_c = L_x/U_b$ are simulated to establish the flow, and statistics (mean and RMS quantities) are obtained over another four convective times.

Figure 3 shows qualitatively the Von-Karman vortex shedding structure in the cold case for both Case A and Case B, in the form of Q-criterion. As expected, smaller structures are obtained for Case B. Figure 2 presents mean and RMS values compared quantitatively with the experimental results[12] for axial and transverse velocities at three different positions $(x_1, x_3, x_5$, see Fig. 1).

Results are in good agreement with the experiments and the two mesh levels (Case A, Case B) produce similar results. Furthermore, we compare the axial mean velocity along x-axis in Fig. 2f. It can be viewed, that the refined mesh (Case B) captures the recirculation zone well. However, the results deviate from the experimental data downstream of the bluff body. This result is believed to be due to the periodic boundaries used on the sides of the wall[21]. In order to check this hypothesis, a simulation is carried out using wall boundaries on the sides at coarser grid $\delta x = 2.0$mm and compared with

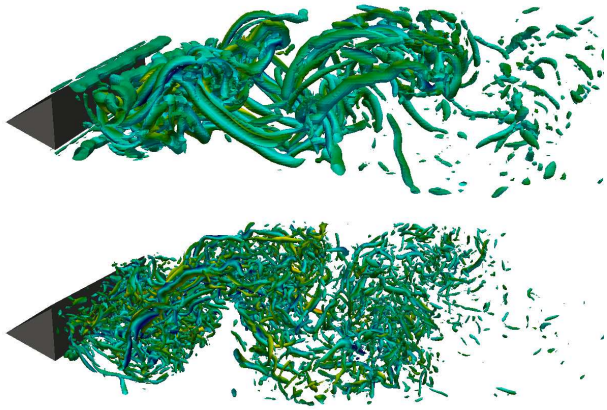

FIG. 3. Vortex shedding pattern for the cold flow. Top: Q-criterion for Case A at 2.0×10^6. Bottom: Q-criterion for Case B at 2.0×10^7

periodic boundaries. Fig. 2.f shows the reduction of this error when wall boundaries are used.

Let us now present the reactive case, with an inlet bulk velocity of 17.3m/s. Following Rochette et al.[22], the parameters related to TFLES model, effective filter and averaging filter widths, are set to $\Delta = 1.4\mathrm{F}\delta_L$ and $\Delta_{avg} = 2.5\Delta$, respectively. Here, δ_L is laminar flame thickness. Note that results report-

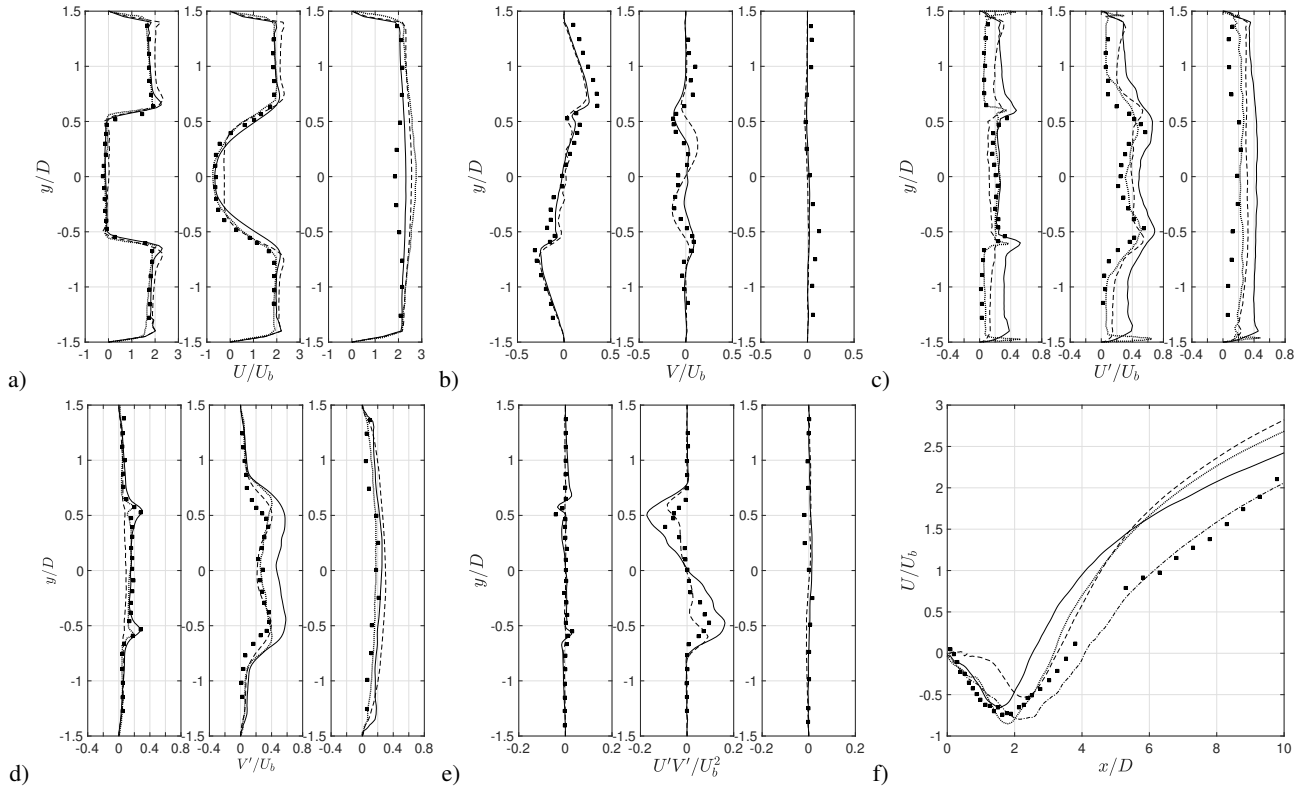

FIG. 4. Quantitative comparisons of our results for the reactive flow, at two different grid definitions, with experimental data at five different points (x_1,x_3,x_5) (from left to right of each sub-figure). a) Mean U profiles. b) Mean V profiles. c) RMS U profiles. d) RMS V profiles. e) RMS UV profiles. f) Mean axial velocity profiles starting from the flame holder. Case A (solid line), Case B (dashed line), experimental data (solid square), reference data - two/step chemistry[22] (dotted line) and reference data - detailed chemistry[22] (dash-dot line)

edly weakly depend on these parameters[22]. The values of flame speed and thickness measured using two/step chemistry on 1D flame at equivalence ratio ($\phi = 0.65$) are 0.2m/s and 0.6mm, respectively. The flame thickening F used in this simulation is 15, corresponding respectively to 4.5 and 9.0 points in the thickened flame for Case A and Case B. The flow field characteristics are altered in the reactive case. The presence of high viscosity and large density ratio compared with cold flow, creates a longer re-circulation zone, and the vortex shedding depicted in Fig. 3 is no longer observed. This is illustrated in Fig. 5, which provides a qualitative illustration of the iso-surfaces at progress variable ($(Y - Y_{fresh})/(Y_{burnt} - Y_{fresh}) = 0.5$) for both Case A and Case B of the reactive flow. Furthermore, we compare in Figs. 4 and 6 the results of mean and RMS values calculated at three different positions (x_1,x_3,x_5) for U, V and $U'V'$, along with temperature profiles measured at x_4,x_4',x_5'. The results are also compared with few available curves in[22].

It can be viewed from the figures that an overall agreement with the experimental and reference data is achieved, we also observe discrepancies between Case A and Case B results. This disparity is then highlighted in Fig. 4.f, where we compare the mean axial velocity profiles along x-axis. The results for finer grid have better agreement just after the bluff body. The recirculation zone is well captured, but the results deviate from the experimental data farther from the flame holder.

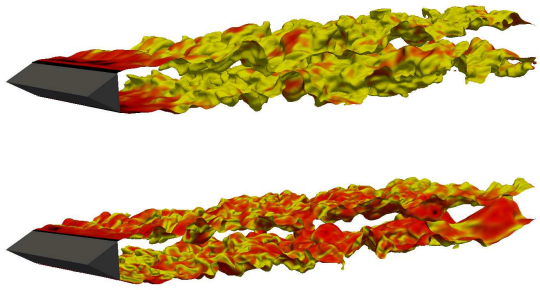

FIG. 5. Iso-surface of the progress variable at 0.5 for the reactive test case (colored by wrinkling factor). Top: Case A. Bottom: Case B

As for the cold flow, this may be partly due to the use of periodic boundaries. Nonetheless, it is also observed that the computed recirculation zone is too short, suggesting that the combustion is too fast. This behavior is known and is reportedly due to the use of a simplified chemistry[22] (see, comparison between detailed and simplified chemistry in Fig. 4.f), an assumption to be lifted in a future study. Furthermore, the errors observed between reference solution, which uses the same TFLES model, may be associated to the interaction of the LB method with the sub-grid models and its dependency

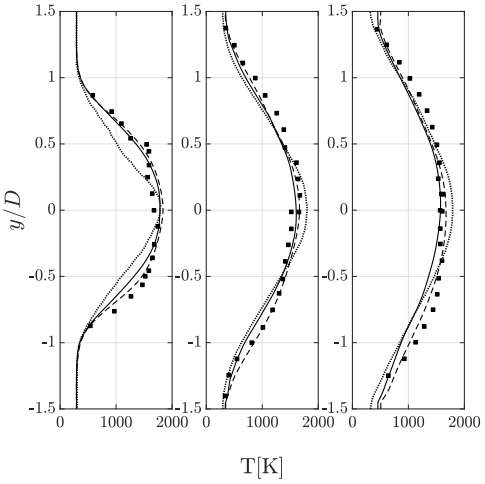

FIG. 6. Temperature profiles at (x_4,x_4',x_5' - left to right). Case A (solid line), Case B (dashed line), experimental data (black solid square) and reference data - two/step chemistry[22] (dotted line)

TABLE II. Computational costs for running a given time ($\approx 7L_x/U_b$) of cold and hot (*) flows, on both meshes (A and B).

Case	N_p	N_c	N_{iter}	T_{sim}	δt	TCPU	RCT	RTTS
A	5.5M	512	0.6M	0.63s	1.06 µs	6 114	6.6 µs	58.2
A*					1.06 µs	7 096	7.7 µs	67.5
B	17.5M	512	1.2M	0.63s	0.52 µs	31 000	5.3 µs	147.6
B*					0.52 µs	36 270	6.2 µs	172.7

on the grid size as reported in[23]. Hence, in order to characterize such discrepancies a thorough research is required into the phenomenon at play. This has been found to be a challenging task, demonstrated by the different results produced by various solvers[23] . Present results remain nevertheless comparable to most reported attempts using LES methods[21,22,32].

Furthermore, Tab. II provides the computational cost for the cold and reacting flow using Reduced Computational Time (RCT) and Reduced Time to Solution (RTTS), computed as:

$$\mathrm{RCT} = \frac{\mathrm{TCPU}}{\mathrm{N_{iter}} \times \mathrm{N_p}}, \qquad \mathrm{RTTS} = \frac{\mathrm{TCPU}}{\mathrm{T_{sim}} \times \mathrm{N_p}}, \tag{9}$$

where TCPU is product of number of cores (N_c) and elapsed time to carry out simulation, N_{iter} is number of iterations, N_p represents number of points and T_{sim} is the physical simulation time. Results are highly encouraging, with about 1000cpuh required to simulate one burner convective time on the coarse mesh.

In conclusion, the first lattice-Boltzmann large eddy simulation of a turbulent premixed flame stabilized in the wake of a bluff-body has been presented. Results are in line with those obtained with classical Navier-Stokes solvers. The reported CPU costs indicate that LBM is an interesting candidate for future LES of combustion processes.

Supplementary material is available for (i) more detail on the pressure-based Lattice-Boltzmann model[10]; (ii) the TFLES filtered equations[22,29] and (iii) the transport and thermo-chemical properties retained for the study[22,29].

B. Rochette is gratefully acknowledged for providing the numerical data associated to his study[22]. The French Space agency (CNES) is acknowledged for supporting Song Zhao at M2P2. Centre de Calcul Intensif d'Aix-Marseille is acknowledged for granting access to its high performance computing resources.

The data that support the findings of this study are available from the corresponding author upon reasonable request.

[1] T. Krüger, H. Kusumaatmaja, A. Kuzmin, O. Shardt, G. Silva, and E. M. Viggen, *The Lattice Boltzmann Method: Principles and Practice* (Springer, 2016).
[2] R. Löhner, "Towards overcoming the LES crisis," International Journal of Computational Fluid Dynamics , 1–11 (2019).
[3] S. Marié, D. Ricot, and P. Sagaut, "Comparison between lattice boltzmann method and navier–stokes high order schemes for computational aeroacoustics," Journal of Computational Physics **228**, 1056–1070 (2009).
[4] Y. Feng, P. Boivin, J. Jacob, and P. Sagaut, "Hybrid recursive regularized thermal lattice boltzmann model for high subsonic compressible flows," Journal of Computational Physics **394**, 82 – 99 (2019).
[5] J. Latt, C. Coreixas, J. Beny, and A. Parmigiani, "Efficient supersonic flow simulations using lattice boltzmann methods based on numerical equilibria," Philosophical Transactions of the Royal Society A **378**, 20190559 (2020).
[6] S. A. Hosseini, H. Safari, N. Darabiha, D. Thévenin, and M. Krafczyk, "Hybrid lattice boltzmann-finite difference model for low mach number combustion simulation," Combustion and Flame **209**, 394–404 (2019).
[7] M. Tayyab, S. Zhao, Y. Feng, and P. Boivin, "Hybrid regularized lattice-boltzmann modelling of premixed and non-premixed combustion processes," Combustion and Flame **211**, 173–184 (2020).
[8] Y. Feng, M. Tayyab, and P. Boivin, "A lattice-boltzmann model for low-mach reactive flows," Combustion and Flame **196**, 249 – 254 (2018).
[9] Q. Li, K. Luo, Q. Kang, Y. He, Q. Chen, and Q. Liu, "Lattice boltzmann methods for multiphase flow and phase-change heat transfer," Progress in Energy and Combustion Science **52**, 62–105 (2016).
[10] G. Farag, S. Zhao, T. Coratger, P. Boivin, G. Chiavassa, and P. Sagaut, "A pressure-based regularized lattice-boltzmann method for the simulation of compressible flows," Physics of Fluids **32**, 066106 (2020).
[11] M. Tayyab, B. Radisson, C. Almarcha, B. Denet, and P. Boivin, "Experimental and numerical lattice-boltzmann investigation of the darrieus-landau instability," Combustion and Flame **221**, 103–109 (2020).
[12] A. Sjunnesson, C. Nelsson, and E. Max, "Lda measurements of velocities and turbulence in a bluff body stabilized flame," Laser Anemometry **3**, 83–90 (1991).
[13] A. Sjunnesson, P. Henrikson, and C. Lofstrom, "Cars measurements and visualization of reacting flows in a bluff body stabilized flame," in *28th Joint Propulsion Conference and Exhibit* (1992) p. 3650.
[14] T. Ma, O. T. Stein, N. Chakraborty, and A. Kempf, "A posteriori testing of algebraic flame surface density models for les," Combustion Theory and Modelling **17**, 431–482 (2013).
[15] D. Maestro, A. Ghani, L. Y. Gicquel, and T. Poinsot, "Les reliability of the volvo bluff-body stabilized ame dynamics," in *55th AIAA Aerospace Sciences Meeting* (2017) p. 1576.
[16] X.-S. Bai and L. Fuchs, "Modelling of turbulent reacting flows past a bluff body: assessment of accuracy and efficiency," Computers & fluids **23**, 507–521 (1994).
[17] I. Porumbel and S. Menon, "Large eddy simulation of bluff body stabilized premixed flame," in *44th AIAA Aerospace Sciences Meeting and Exhibit* (2006) p. 152.
[18] X.-r. Zou, H.-l. Pan, Z.-w. Huang, and F. Qin, "Large eddy simulation of bluff-body stabilized turbulent premixed flame based on openfoam," in *Ninth Mediterranean Combustion Symposium* (2015).
[19] C. Fureby and S.-I. Moller, "Large eddy simulation of reacting flows applied to bluff body stabilized flames," AIAA journal **33**, 2339–2347 (1995).

[20]N. Zettervall, K. Nordin-Bates, E. Nilsson, and C. Fureby, "Large eddy simulation of a premixed bluff body stabilized flame using global and skeletal reaction mechanisms," Combustion and Flame **179**, 1–22 (2017).
[21]H. Wu, P. C. Ma, Y. Lv, and M. Ihme, "Mvp-workshop contribution: Modeling of volvo bluff body flame experiment," in *55th AIAA Aerospace Sciences Meeting* (2017) p. 1573.
[22]B. Rochette, F. Collin-Bastiani, L. Gicquel, O. Vermorel, D. Veynante, and T. Poinsot, "Influence of chemical schemes, numerical method and dynamic turbulent combustion modeling on les of premixed turbulent flames," Combustion and Flame **191**, 417–430 (2018).
[23]P. A. Cocks, M. C. Soteriou, and V. Sankaran, "Impact of numerics on the predictive capabilities of reacting flow les," Combustion and Flame **162**, 3394–3411 (2015).
[24]V. Chakravarthy and S. Menon, "Large eddy simulations of confined bluff body stabilized highly turbulent premixed flames. asme fluids engineering summer meeting paper no," Tech. Rep. (FEDSM-99-7798, 1999).
[25]J. Jacob, O. Malaspinas, and P. Sagaut, "A new hybrid recursive regularised bhatnagar–gross–krook collision model for lattice boltzmann method-based large eddy simulation," Journal of Turbulence , 1–26 (2018).
[26]T. Poinsot and D. Veynante, *Theoretical and numerical combustion* (RT Edwards, Inc., 2005).
[27]A. Vreman, "An eddy-viscosity subgrid-scale model for turbulent shear flow: Algebraic theory and applications," Physics of fluids **16**, 3670–3681 (2004).
[28]S. Wilhelm, J. Jacob, and P. Sagaut, "A new explicit algebraic wall model for les of turbulent flows under adverse pressure gradient," Flow, Turbulence and Combustion , 1–35 (2020).
[29]B. Rochette, E. Riber, B. Cuenot, and O. Vermorel, "A generic and self-adapting method for flame detection and thickening in the thickened flame model," Combustion and Flame **212**, 448–458 (2020).
[30]F. Charlette, C. Meneveau, and D. Veynante, "A power-law flame wrinkling model for les of premixed turbulent combustion part i: non-dynamic formulation and initial tests," Combustion and Flame **131**, 159–180 (2002).
[31]F. Charlette, C. Meneveau, and D. Veynante, "A power-law flame wrinkling model for les of premixed turbulent combustion part ii: dynamic formulation," Combustion and Flame **131**, 181–197 (2002).
[32]A. Ghani, T. Poinsot, L. Gicquel, and G. Staffelbach, "Les of longitudinal and transverse self-excited combustion instabilities in a bluff-body stabilized turbulent premixed flame," Combustion and Flame **162**, 4075–4083 (2015).
[33]A. Smirnov, S. Shi, and I. Celik, "Random flow generation technique for large eddy simulations and particle-dynamics modeling," J. Fluids Eng. **123**, 359–371 (2001).